Redox geochemistry of the Riddlesburg Shale Member, Rockwell Formation: Trace metal enrichment in seawater and sediments following basal Carboniferous glaciation

Justus McMillan

Advisors: Profs. A. Jay Kaufman (UMD) and Geoffrey Gilleaudeau (GMU)

GEOL 394

Table of Contents

Abstract

This study consists of a sedimentological and geochemical analysis of the Riddlesburg Shale Member, a potential boundary marking the transition from Late Devonian to the Early Carboniferous within the stratigraphy of the Appalachian foreland basin. The glacial mobilization of nutrients, reductive agents, and trace metals from the Acadian highlands are postulated to have affected the microbial communities within the Appalachian Basin. The changes to redox conditions within the basinal waters may have been syn-depositional with the transport of material by glacial and fluvial processes. The biogeochemical changes occurring with the Appalachian foreland basin are compared with the coeval upper Bakken Formation black shale of the Williston Basin in southwestern Canada and northwestern USA. The Bakken shale, a major oil and natural gas producer for the USA, provides a window into mid-Paleozoic anoxia in epicontinental seaways that is suggested as the cause of mass extinctions. Interpretations of the Bakken shale geochemical data suggests an expansion of marine euxinia (free H_2S in the water column) during transgressive phases that affected the function of anaerobic microbes reflected in changes in stable isotope (C, N, and S) compositions of seawater proxies, as well as the processes whereby trace metals such as Mo and V are removed from the water column and sequestered into sediments. The Riddlesburg Shale Member (RSM) core data suggests the Appalachian Basin was an oxic environment with low total organic carbon (TOC) and not as enriched in trace metals as the Bakken Shale.

Introduction

Anoxia and Extinction

Recessions of glacial ice followed by intervals of widespread water column anoxia during transgressions occurred several times in Earth history. The Late Devonian is characterized by several key, and at the time, emergent events in Earth history. During this period, two or possibly more, mass extinction events occurred. These mass over-turnings of the Devonian biota have been grouped together as one of the five major mass extinctions of the Phanerozoic eon (Sepkoski, 1979). A well-studied pulse within this Late Devonian mass extinction occurred at the terminal Frasnian (372.2 Ma) and is known as the Kellwasser event. The event is named after the Kellwasser Kalke beds in the Harz Mountains in Germany (Roemer, 1850; Carmichael et al., 2019). Within the Kellwasser Kalke section, two black shales separated by a layer of limestone define an Upper and Lower Kellwasser Event (Camichael et al., 2019). This black shale, which is the type section of the Kellwasser, is characterized by a positive $\delta^{13}C$ excursion. The second extinction pulse occurred at the terminal Famennian (358.9 Ma) and is referred to as the Hangenberg event. In addition to anoxic conditions, this event is associated with sea-level change. Like the Kellwasser, this event is named after a black, organic-rich marine shale (Caplan & Bustin, 1999). The Hangenberg Shale is a part of the synchronous global continuum of other black shales that illustrate the extent of anoxia into several paleoenvironments (Feist, 1990; Caplan & Bustin, 1999). It is proper to refer to the event as a global occurrence given that black shales covered 21% of depositional area in the Famennian (Caplan & Bustin, 1999).

The Late Devonian benthic and reef building biota experienced severe loss during the Frasnian and onward into the Devonian-Carboniferous transition, with 97% of shallow water and 60% of deep-water rugose coral species going extinct during the Kellwasser event (Barash, 2015; 48), also coinciding with the decline in 80% of Tabulate coral genera during the same crisis (Barash 2015). During this event 33 families of Devonian brachiopods, with representatives of 30 of them being tropical dwelling species (Barash, 2015). Potentially the grisliest of losses from the Frasnian to the Devonian-Carboniferous transition is expressed by the decline of the stromatoporoids. The stromatoporoids were the main reef builders during the Frasnian (Barash, 2015; Algeo & Berner, 1995); however, 50% of stromatoporoid families were lost by the end of the Frasnian. While calcareous algae claimed the ecological position of main reef-builder the remaining stromatoporoids were relegated to colder, benthic environments (Barash, 2015). The window of extinction for stromatoporoids is debated within the community. Potentially they disappear at the end-Frasnian boundary marked by the Kellwasser event (Stock, 2005), or are heavily culled by the Kellwasser and ultimately annihilated during the subsequent Hangenberg event (Barash, 2015). Perhaps the *Labechia carabonaria* Smith 1932 discovered in Lower Carboniferous strata (Smith, 1932) represents a Lazarus taxon and the stromatoporoids survived just barely into the Carboniferous (Kershaw 2020).

Figure 1. A reconstruction of what a Devonian reef environment may have looked like prior to the collapse of the reef-building biota of the period (John, 2007).

The disappearance of these major reef-builders, such as the stromatoporoids in the Late Devonian marine environment occurs alongside the changes in sea levels and major excursions in the sedimentological and geochemical records (Algeo et al., 1995). Anoxia in these environments is expressed by laminated black shales indicating widespread oceanic anoxia, the deposition of organic-rich shales and coal, and the positive excursions in $\delta^{34}S$ caused by large-scale bacterial sulfate reduction (Algeo et al., 1995). This is all preceded by a period of cooling and glaciation during the Late Devonian, one that may be spurred by the inception of vascular land plants.

The Emergence of Embryophytes

Embryophytes (Land plants) have evolved from charophycean green algal ancestors (Becker & Marin, 2009). Although land plants likely arose in the Early Ordovician, they were small and did not have the global effect they would later have in the Late Devonian. Even by

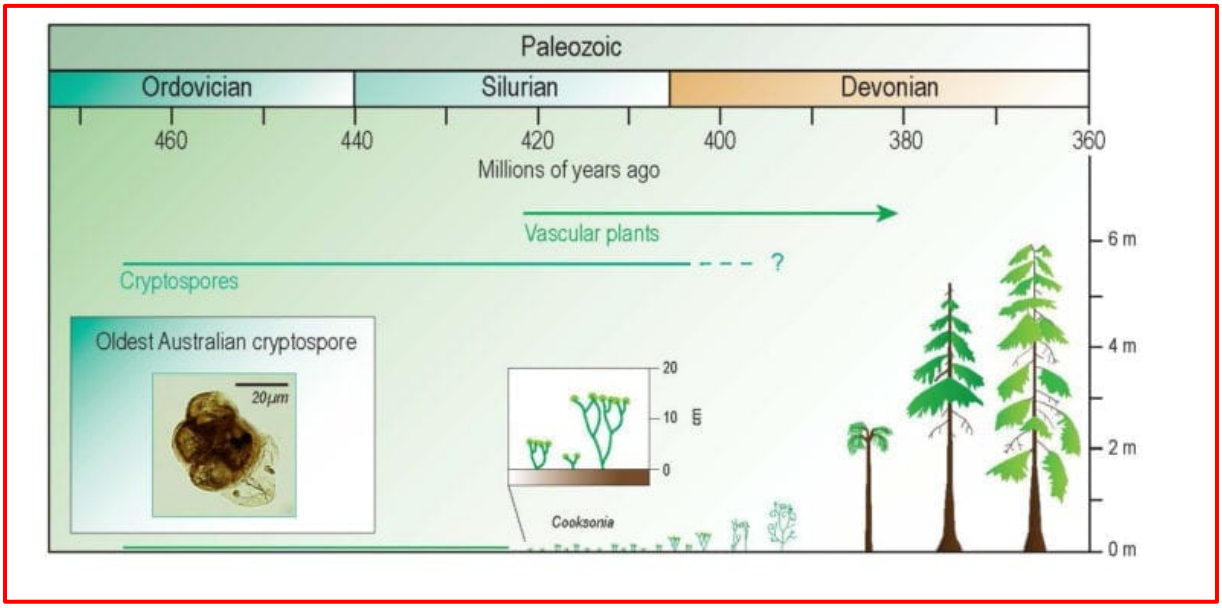

Figure 2. Figure depicting a time series of plant growth from the Ordovician to the Late Devonian. Notably, these plants grow exponentially between the geological periods. Modified from Spaak (2017).

Late Silurian, plant sizes were only around 3 mm in diameter (Raven & Edwards, 2001). The first vascular plants would take more than 20 million years to evolve (Pawlik et al., 2020). The first known example of these early vascular land plants is *Cooksonia* (Lang, 1937; Edwards et al., 1992). Many of these early vascular plants would have been restricted to moister environments initially, then were able to radiate further onto the continent. The larger Late Devonian vascular plants, with more complex root systems, are theorized to have impacted both physical and chemical weathering of the continents. Continental rock-derived elemental nutrients such as P, K, Fe, Mg, and N (Raven & Edwards, 2001) were then taken up by plants and concentrated into the soil. Devonian land plants would have affected the climate and oxygenation state of the Earth by the photosynthetic uptake of CO_2, which would be stored as wood cellulose, and the release of O_2 to the atmosphere.

By the Middle Devonian, several groups of vascular land plants exhibited increased arborescence (tree-sized stature) and seed habits enabling their conquest of the terrestrial environment (Algeo et al., 1995; Chaloner & Sheerin, 1979; Mosbrugger, 1990). The relationship between periods of oceanic anoxia and the size and development of land plants may express a positive correlation in which these organisms did heavily affect the global environment. Secondary vascular supporting tissues develop around the onset of Middle-Late Devonian marine anoxia, coinciding with the size increase of the land plants (Algeo et al., 1995). Seeds precede the Hangenberg event by one conodont zone, or approximately 0.5 m.y. (Algeo et al., 1995; Gillespie et al., 1981; Rothwell et al., 1989). While the demise of the Devonian reef

community is ever present during this time, the Devonian arboreal community rises to prominence as a new environmental force that interacts with the geochemistry of the soil substrate and the Devonian atmosphere.

Paleogeography

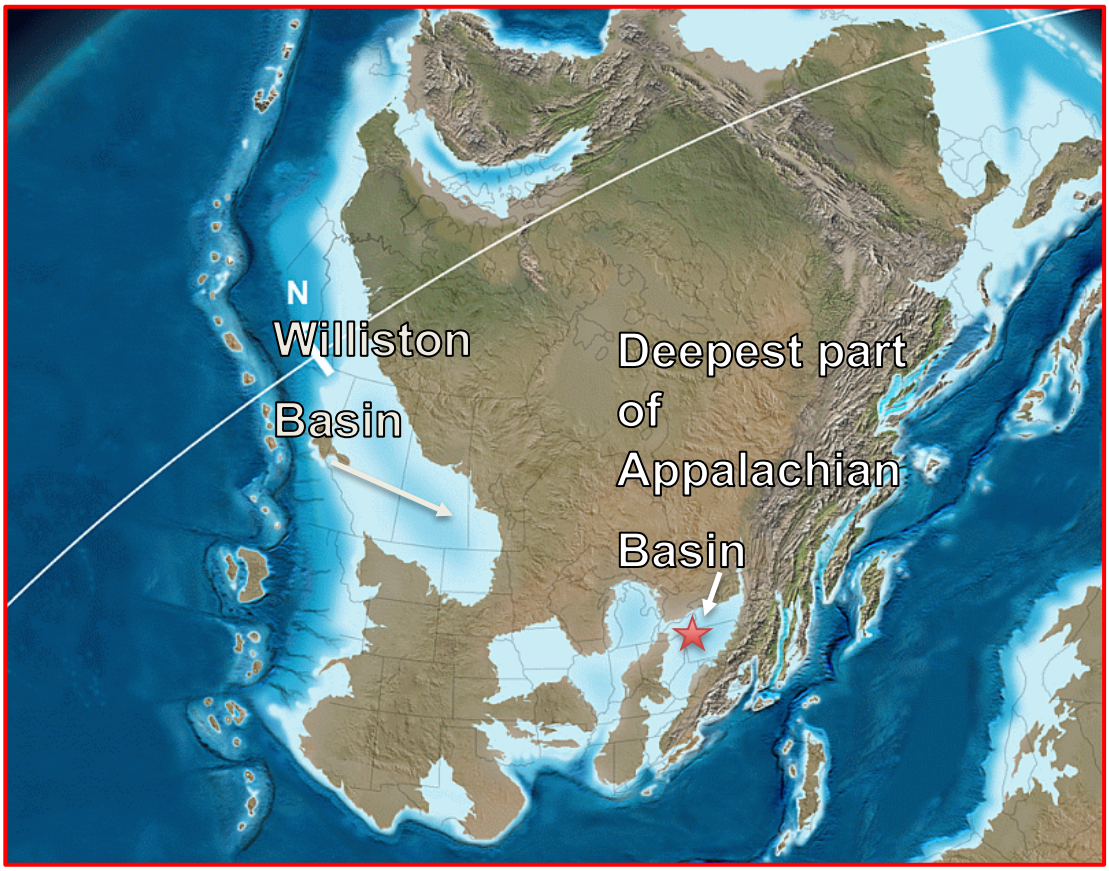

Figure 3. Reconstruction of Late Devonian Laurentia. From Blakely (2016)

Williston Basin

The Williston Basin occupies 110,000 square miles in the states of North Dakota, South Dakota, and eastern Montana (Sandberg, 1962). The Williston Basin did not experience the amount of tectonism that is observable in the Appalachian Basin. This basin exists as a flat to gentle rolling plain (Sandberg, 1962). Sedimentary layers corresponding to each of the period within the Phanerozoic has been deposited within the basin. The Bakken Formation of the Williston Basin is contemporaneous with the Riddlesburg shale of the Appalachian Basin but has a different tectonic history. The western Laurentian margin was subjected to the Antler orogeny of the late Devonian that continued into the Early Pennsylvanian. The deposition of the Bakken shale occurred during a transgression period (Ketner, 2013). The rising sea level would have caused a stratification of the water column and would have created an anoxic bottom surface condition amenable for the accumulation of organic material.

Appalachian Basin

Initial formation of the Appalachian Basin was brought about by the tectonic activity associated with the Taconic orogeny. This orogeny was underway during the Early Ordovician (480 Ma) and began to envelop the eastern margin of Laurentia with landmasses like microcontinents and volcanic arcs (Faill, 1997). The collision between the carbonate shelf (Faill, 1997) and islands created the Taconic highlands and the foreland basin to the west of the mountains. After the erosion of Taconic highlands, the eastern margin regressed to a carbonate shelf again. The following Acadian orogeny began at 440 Ma during the Silurian. During this event, the landmasses of Avalonia and Baltica slammed into eastern Laurentia to form the Acadian highlands. The orogeny help facilitate the deposition of clastic material into the foreland basin.

The Effect of Embryophytes on Atmospheric CO_2

The drawdown of atmospheric pCO_2 during the Devonian had far-reaching climatic consequences, contributing to global cooling and a short Late Famennian glacial episode (Algeo & Scheckler, 1998). The evidence of a cooling period and glaciation during the Late Devonian have been interpreted from high latitude areas of Gondwanaland where glacial deposits are widespread (Brezinski et al., 2008). Figure 3 shows a paleogeographic reconstruction of Devonian continental masses. There are assumptions that continental glaciation would have occurred at latitudes greater than 70 degrees (Frakes et al., 1992) and the potential of glacier formation at a minimum of 55 degrees (Isaacson & Sadlock, 1900). It seems like a likely cause for the glaciation is the drawdown of atmospheric CO_2 by land plants, and by the burial of photosynthetically derived organic matter in the oceans. These events were enhanced by the chemical weathering that may have led to the increased deposition and fluxes of different nutrient that promoted development of eutrophic conditions in epicontinental seaways, resulting in algal blooms, widespread bottom water anoxia, and high sedimentary organic carbon fluxes (Algeo & Scheckler, 1998). Long-term effects included drawdown of atmospheric pCO_2 and global cooling, leading to a brief Late Devonian glaciation (Brezinski et al., 2008), and setting the stage for icehouse conditions observable in the Carboniferous.

Figure 4. The Rockwell Formation diamictite (orange star) and Riddlesburg Shale Member (blue star) outcrop located at Sideling Hill, along I-68 in Maryland.

Deposition of the Rockwell Diamictite and the Effect on Alkalinity

Below the Riddlesburg Shale Member lies a Late Devonian polymictic diamictite deposited over 400 km from

northeastern Pennsylvania to western Maryland and into east-central West Virginia (Brezinski et al., 2008). A diamictite is a poorly sorted or non-sorted terrigenous non-calcareous sedimentary rock that contains variably sized clasts from clay to boulders in a muddy matrix (Flint et al. 1960). This diamictite is likely glaciogenic in genesis, and this is supported by examination of the unique lithology exhibited. Brezinski et al., (2008) describe this diamictite as a matrix-supported, unbedded, locally sheared deposit. It contains subangular to rounded clasts up to 2 m in diameter. Interesting to note, the clasts seem to be both locally derived from surrounding lithologies and exotic (Brezinski et al., 2008). Two agents of transport are the likely vehicles that the unlithified sediment was deposited by, into the foreland basin.

Figure 5. Magic-Gigapans Group, cross section of polymictic Rockwell diamictite. The clasts are poorly sorted and subrounded to rounded. The roundness of these clasts would suggest a prolonged subjection to abrasion of the grains during transportation.

Glaciers on the Acadian highlands could have sheared mass amounts of material from the mountains and deposited them into the Appalachian Basin. This claim can be supported by an examination of the clasts within the diamictite. Many of them display these physical marks (see Fig. 5). They are striated and faceted, and this is a common property of clastic material that has been moved by glacial activity. This is significant because the polymictic diamictite in the Rockwell Formation beneath the Riddlesburg Shale Member is the only lithological evidence of glaciation occurring in Laurentia. Again, the other factor that this assumption is based off is also the variety in clast and mineral type, as well as the presence of multiple striation directions (Brezinski et al., 2008). Igneous and metamorphic clasts exist within the diamictite (see Fig. 4)

that are not of a definitive source but would have been transported at least 100-120 km. This mixing of local and exotic clasts is common in glacial deposits (Brezinski et al., 2008).

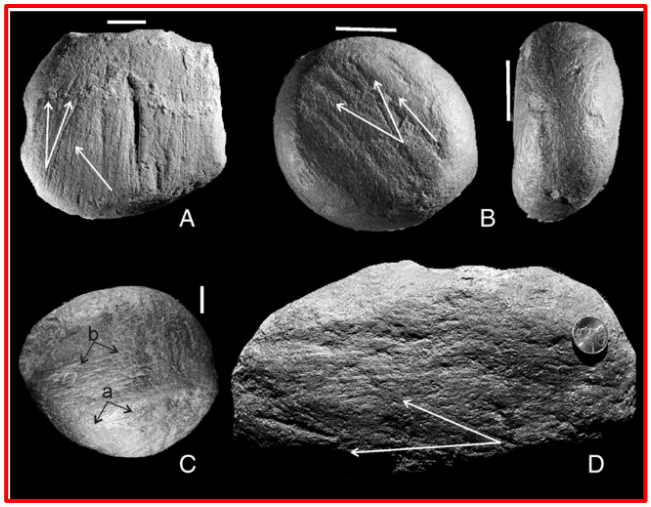

Figure 6. A depiction of the multidirectional striations suffered by clasts that were in the Rockwell diamictite matrix. This is evidence for glacial activity in Southern Laurentia. From Brezinski et al. (2008).

The burial of both organic carbon and calcium carbonate are pathways for carbon removal from the atmosphere and hydrosphere reservoirs (Milliman, 1993), the Appalachian Basin likely received a large influx of organic carbon shed off the continent by glaciation of the Acadian highlands. This deposition of nutrients would spur the microbial sulfate reducers into producing alkalinity as a byproduct of their metabolism (Torres, 2020). These microbes would not only utilize the sulfate introduced to the basin but also the iron other nutrients. The weathering of silicate minerals exposed on land also generates alkalinity and dissolved ions (Torres, 2020).

In the terminal Devonian strata of Maryland and Pennsylvania, the Riddlesburg Shale Member, a black shale, overlies marine sheet sands and a glacial diamictite of the Rockwell Formation, which is likely to be basal Mississippian in age (358.9 Mya). The Rockwell diamictite may represent the only direct evidence of an early Carboniferous ice age deposit in Laurentia and given paleogeographic reconstructions there may have been glacial ice at or near sea level within 25 degrees of the equator (Brezinski et al., 2008). The upper Bakken Shale of the Williston Basin similarly overlies a marine sandstone, a sea level low sand deposit that is a likely equivalent to the Rockwell diamictite. Insofar as equivalent shale deposits in the Appalachian and Williston Basins in the United States are known to be enriched in both organic matter and trace metals, this study seeks to understand basinal redox conditions to better understand whether post-glacial weathering processes resulted in the delivery and sequestration of additional metals and organic carbon in the Riddlesburg Shale Member.

Hypotheses

1. The glacial mobilization of nutrients, sulfate, alkalinity, and trace metals from the Acadian highlands into the Appalachian foreland basin affected biogeochemical processes and spurred anoxic and potentially euxinic (free H_2S in the water column) conditions across the Devonian-Carboniferous transition.
2. Changes to redox conditions affected the sequestering of redox sensitive trace metals (RSTMs) in the organic rich foreland Appalachian Basin sediments.

Null hypothesis

The Riddlesburg Shale Member (RSM) does not display similar concentrations of organic carbon or RSTM, compared to the Bakken shales. The Appalachian Basin was then not as anoxic as the Williston Basin, and lacked the euxinic conditions necessary for RSTM hyper-enrichment.

Background

Bakken Shale

The Bakken Formation of the Williston Basin in southwestern Canada and northwestern USA is 10,868 ft. below surface. It consists of three units: The Lower Bakken (LB), Middle Bakken (MB), and Upper Bakken (UB). LB and UB are both organic rich black shales; MB is a mixed carbonate-siliciclastic deposit. The Bakken Formation has become one of the most import sources of crude oil production for the USA in the last few decades (Nicas, 2012). Record oil extraction from the Bakken Formation began in 2006, substantial economic boom in North Dakota transpired from 2006 to 2012 (Englund, 2020).

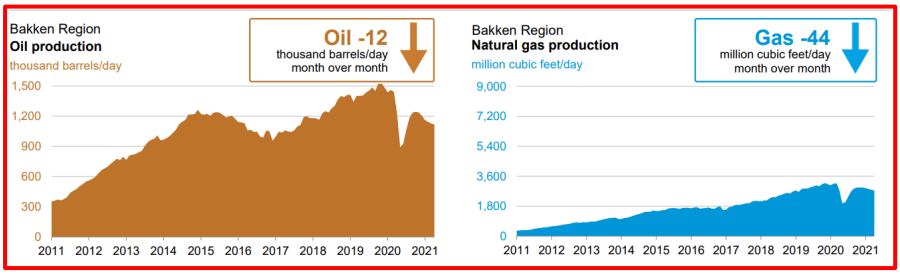

Figure 7. The oil and natural gas production from the Bakken Formation. In 2019 the region produced over 1,500,000 barrels of oil a day, making it one of the most important regions for oil production in the USA. The data is sourced from the Drilling Productivity Report from the U.S. Energy Information Administration.

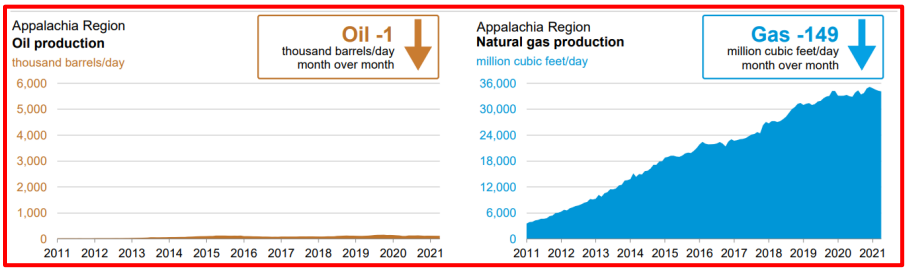

Figure 8. The oil and natural gas production from the Bakken Formation. The data is sourced from the Drilling Productivity Report from the U.S. Energy Information Administration. The oil production of the Appalachian Region is eclipsed by the Bakken Region while the natural gas production is the opposite.

For the scope of this study the UB is especially of interest as it presents a coeval deposit of shale that is associated with post-glacial transgression. The Riddlesburg Shale Member (RSM) of the Appalachian Basin could thus represent a comparable environment where anoxic conditions may have stimulated microbial sulfate reduction in the water column and resulted in the sequestration of trace metals and organic carbon.

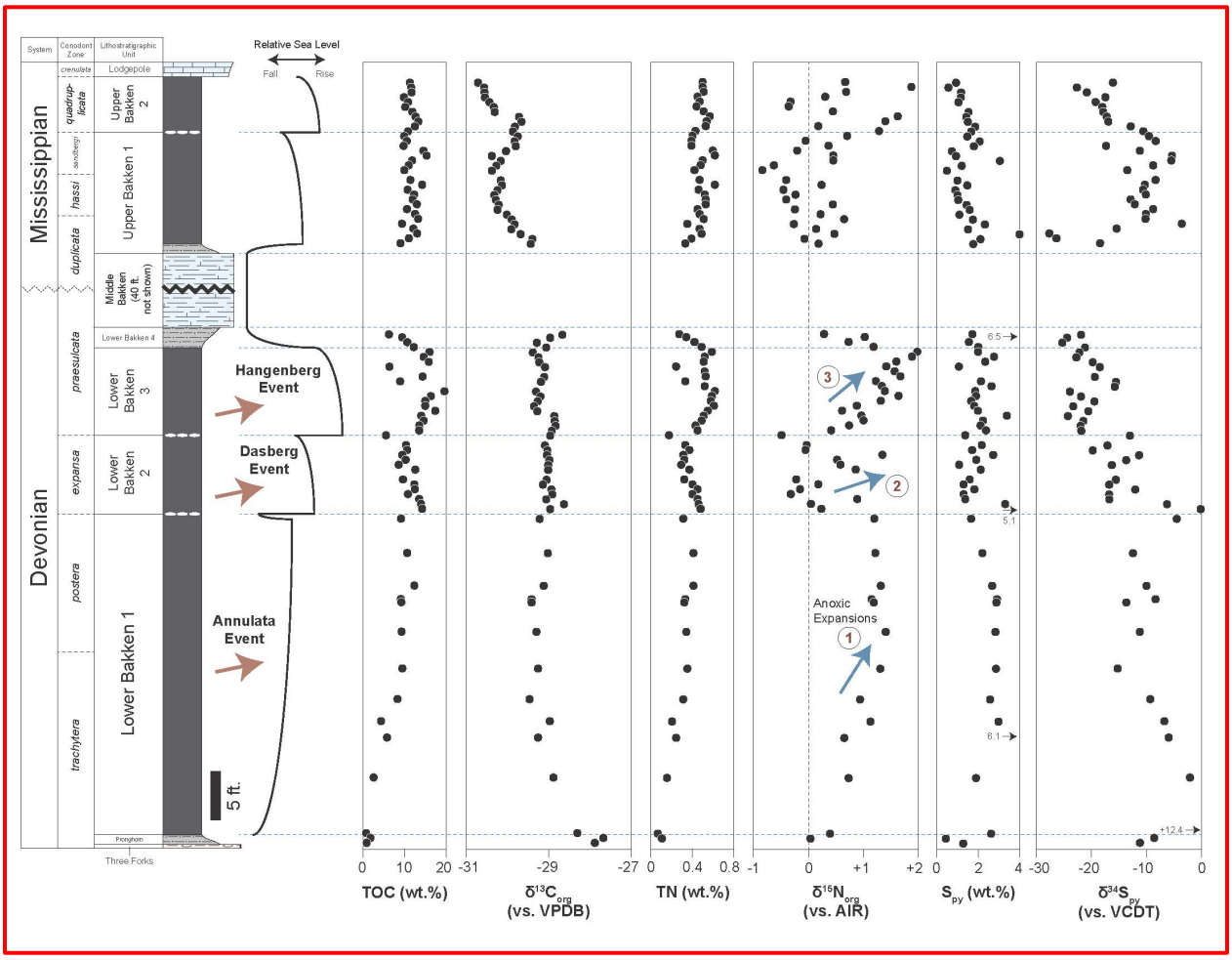

Figure 9. Time-series geochemical trends through the Lower, Middle, and Upper Bakken units. These samples were analyzed for the abundance of TOC, total nitrogen (TN), and total S_{py} (TS), as well as their carbon, nitrogen, and sulfur isotope analyses completed to date. The data is posted against the stratigraphy of the Bakken units and displays correlative change in relative sea level of the Williston Basin. The Annulata, Dasberg, and Hangenberg extinction events are also shown, all of which coincide with the falling of relative sea level and isotopic trends in the data.

Carbon (C)

The $\delta^{13}C_{org}$ in LB1 gradually decrease from -27‰ to -29‰, these values become invariant around -29‰ for the rest of the LB1 stratigraphy. LB2 $\delta^{13}C_{org}$ values trend more positively at the base of the unit but return to the invariant -29‰ values recorded closer to the summit of the LB1 unit. There is a correlation between relative sea level rise and the positive excursions in $\delta^{13}C_{org}$. This correlation continues in the LB3 unit, and Hangenberg event similarly marks a decrease in sea level just how the Annulata and Dasberg events of LB1 and LB2 respectively did. The LB4 unit trends differently than the other Lower Bakken units, recording a positive excursion in $\delta^{13}C_{org}$ values with the sharp decline in relative sea level faced. Siltstone represents the lithology of the LB4 unit. These $\delta^{13}C_{org}$ values may display less negatively in the chemostratigraphy due to the dilution of imposed by silicate weathering occurring. $\delta^{13}C_{org}$ deviate from -29.5‰ at the base of the UB1 to <-30.5‰ at the top of the unit, UB2 $\delta^{13}C_{org}$ show invariance then trend negatively as the relative sea level lowers again. Average means of -29‰ are the typical baselines for Paleozoic marine $\delta^{13}C_{TOC}$ are -29‰ (Martinez, 2018).

Nitrogen (N)

Ammonium and nitrate are used as N sources in primary productivity (Liu et al., 2016) and the respective fractionations are − 10(± 5)‰ and − 3(± 2)‰ (Liu et al., 2016; Hoch et al., 1994; Waser, 1998). Denitrifiers, which are also aerobic respirers switch to these N sources as electron acceptors for anaerobic respiration when oxygen is depleted (Ward, 2012). The fluctuation of $\delta^{15}N_{org}$ gives an idea of how productive the microbial communities were and perhaps how transgressional phases effected the Williston Basin. The first three Lower Bakken units have positive $\delta^{15}N_{org}$ excursions which correlate with the end of the extinction events and the drop in relative sea level (Fig. 8). Denitrification increased at the end of the LB1, 2, and 3. These positive excursions indicate a depletion of the lighter ^{14}N from the water column. The gaseous N_2 would have been enriched in ^{14}N and released to the atmosphere, while the residual nitrate in the Williston Basin would be enriched in the ^{15}N isotopes. LB4 $\delta^{15}N_{org}$ values trend closer to zero. Upper Bakken $\delta^{15}N_{org}$ values are oscillate between -1 to 1‰ in UB1, a positive excursion towards +2‰ in UB2 records another anoxic expansion like the ones in the Lower Bakken units.

Sulfur (S)

Trends in $\delta^{34}S$ coincide with the sea level; LB1, LB2, and LB3 are records of a gradual negative excursion from 0 to -30‰ (Fig. 8). Dips in the relative sea level coincide with less negative $\delta^{34}S$ values. A fall in relative sea level would then mean a restriction of water flow, and a decrease in the amount of sulfur present Williston Basin as a result. The average relative sea level increases from the LB1 to the LB3 unit, therefore this may provide a reason for the increasingly negative values shown in the Lower Bakken. Relative sea level remained high enough for a sizeable sulfur reservoir to build up within the Williston Basin, fueling the sulfate reducers present. UB1 and UB2 record a similar correlation between the relative sea level and the size of the sulfur reservoir, based upon the activity of microbial sulfate reducers.

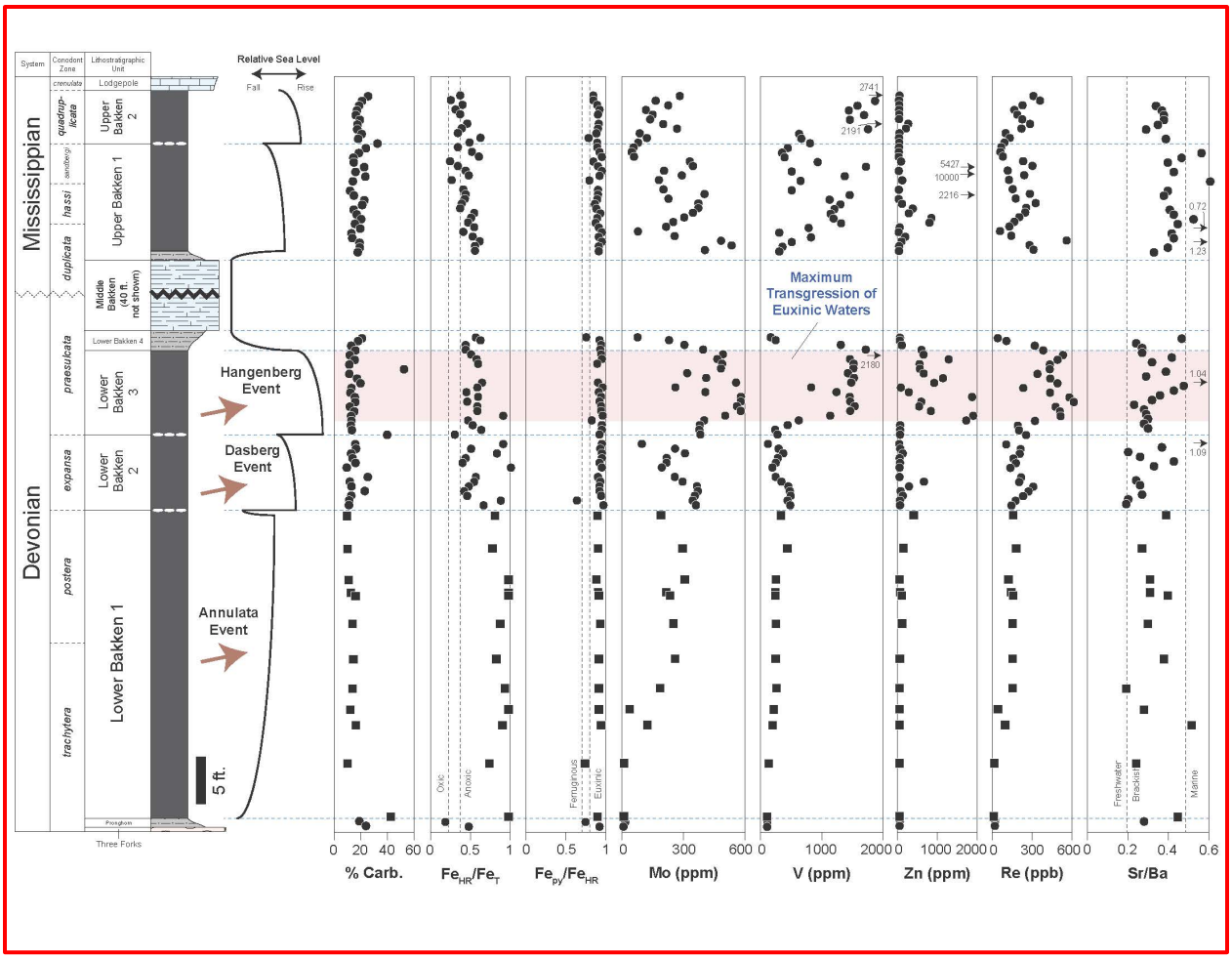

Figure 10. Time-series geochemical trends through the Lower, Middle, and Upper Bakken units. These samples were analyzed for the abundance of trace metals such as Mo, V, U, and Re in the Bakken units during a period of decline in the intensity of euxinic conditions of the Williston Basin, completed to date. The data is posted against the stratigraphy of the Bakken units and displays correlative change in relative sea level of the Williston Basin. The Annulata, Dasberg, and Hangenberg extinction events are also shown, all of which coincide with the falling of relative sea level and isotopic trends in the data.

Percent carbonate

The percentage of carbonate present in the Lower Bakken (LB) trends as more abundant than the Upper Bakken (UB) carbonate inventory. Initial assumptions should be focused on the change in relative sea level and how this may affect the carbonate inventories of both Bakken units. Low stands in the basin's history signify a closing of the system and the restriction of geochemical reactions that would otherwise occur during low stand. The rise of relative sea level may have promoted the transference of acidity from the open ocean into the Williston Basin. this may be a result of change in the alkalinity within the Williston Basin. Perhaps the concentration of Ca^{+} ions is related to sea-level change. Aside from two distinct outliers within the LB stratigraphy, carbonate deposition is low as w effect on carbonate percentage within the shale is observable. The UB exhibits gradual increase in the percent carbonate present in its

stratigraphy. Calcium carbonate nucleation and growth kinetics are affected by different operating conditions (Korchef & Touaibi, 2019). The saturation of Ca^{+} ions within the water column, pH, temperature, and presence of foreign ions play a crucial role in the synthesis of carbonates and their deposition (Korchef & Touaibi, 2019).

Molybdenum (Mo)

Molybdenum is sourced to oceans by oxidative weathering of continental crust Mo sediment enrichment is abundant within a marine environment when a lack of O_2 is the condition of the seawater (Emerson & Huested, 1991; Calvert & Pederson, 1993). H_2S present in bottom waters would provide the euxinic conditions for Mo to accumulate in higher concentrations that are observed in both the UBS and LBS (Scott et al., 2017). Mo concentrations are extremely low in LB1 but grow to an average of 300ppm halfway through the stratigraphy. Concentrations dip along with the falls in relative sea level, this is reminiscent of what is observed from the trends in the CNS data presented by figure 8. LB3 has the highest rise in relative sea level present in the Bakken and this is where the largest Mo concentrations are recorded, reaching 600 ppm (Fig. 9). Mo concentrations in the Upper Bakken units begin with similar concentrations to LB3 but slowly decrease to <300 ppm. If Mo concentrations of 25-100 reflect an environment that was either intermittently euxinic or extremely restricted (Scott et al. 2008) then the over 600ppm concentrations found within the LBS (Scott et al. 2008) is an indication of extremely euxinic conditions within the Williston Basin. UBS concentrations reflect waters that would have been weakly to moderately euxinic.

Vanadium (V)

V is another redox sensitive trace element that was present in the Williston Basin at the time of the Bakken shale's deposition. V (III) is an oxidation state of the element that occurs under strongly reducing conditions (Gustafsson, 2019). V (IV) is another state of V that occurs and is stable at low pH, mildly reducing conditions, and this is particular to high concentrations of organic matter (Gustafsson, 2019) in bodies of water. V concentrations gradually increase from LB1 to LB2 like the Mo concentrations. V seems to be hyper enriched in the LB3 unit, coinciding with the maximum transgression of the euxinic waters of the Williston Basin. The concentration in LB4 is severely reduced in comparison to the LB3 hyper enrichment. UBS V concentration increased drastically from the UB1 to UB2 unit, UB2 has V hyper concentrations of <3000 ppm, greater than what is observed in the LB3 transgressional maximum.

Anti-correlation of Mo and V in the Upper Bakken shale (UBS)

Trace metal concentrations of Mo and V display an anti-correlated trend within the Williston Basin's stratigraphy. Initial Mo abundance in the UBS is near zero but in a short geological timespan reach concentrations of over 600 ppm. Thereafter, Mo concentrations are much high during the early stages of the UBS deposition but decrease over 50% in total abundance moving up the stratigraphy, towards the Lodgepole Fm. The concentration of V within the UBS sediments exhibits a gradual increase from near zero ppm to nearly 3,000ppm before the transition to the Lodgepole. 10,787 feet is the approximate depth correlating to V concentrated in sediment of the UBS an order of magnitude more abundantly than Mo. The anti-correlation between Mo and V is a product of the Williston Basin redox conditions after the transgressional change from the carbonate-siliciclastic Middle Bakken unit described by

Egenhoff to the UBS. Euxinic conditions of the Williston Basin lessen moving up the stratigraphy but the basin remains euxinic for the entirety of the UBS depositional sequence.

Vanadium enrichment in many ancient marine organic-rich shales is recorded as >500 ppm (Kunert, 2020). Molybdenum is a redox sensitive trace metal found to enrich sediment under similar environmental conditions required for V sequestering and enrichment (Kunert, 2020), yet an anti-correlation in abundances is recorded in the consistently euxinic UBS unit. The interactions between other inorganic compounds and organic material with Mo and V in the water column might explain this anti-correlation. $V^{(III)}$ forms a solid solution series with $Fe^{(III)}$ in oxides (Kunert, 2020) and with Al in clays (Kunert, 2020; Breit & Wanty, 1991). The Vanadyl oxocation VO^{2+} has a strong affinity for surface adsorption to solid particulates (Kunert 2020); this includes inorganic oxide phases (Al_2O_3 and TiO_2) (Kunert, 2020; Breit & Wanty, 1991) and organic molecules (humic, fulvic, and carboxylic acids) (Kunert, 2020; Gustafsson, 2019; Breit & Wanty, 1991). While Mo reacts with H_2S to form Mo-sulfides which then further interact with H_2S (Erickson & Helz, 2000), V interacting with H_2S does not produce V-sulfides or V-bearing Fe-sulfides (Kunert, 2020; Algeo & Maynard, 2004). Mo and V anti-correlation in the Bakken shale and the negative $\delta^{13}C$ excursion may have been enabled by an influx in ^{13}C depleted material to the basin. Rising sea levels would have opened the Williston Basin to photosynthesizers, or a greater abundance if they were present before. Fractionation by plankton results in a carbon isotopic composition depletion in water column (Maslin & Swann, 2006) and would then impact what C isotopes would then be available for the Mo and V.

Methods

Physical preparation

The samples of the Riddlesburg Shale Member used in this study have been provided by the Pennsylvania Geological Survey (PAGS). John Neubaum State geologist of the PAGS was the correspondent that helped retrieve these core samples from the PAGS shed storage. The cores were drilled as a part of a project to expand upon what was known about the geology of Ohiopyle State Park in southwestern Pennsylvania. For the scope of this current project, the cores will be used gain a better understanding of the redox conditions of the Appalachian Basin during transition from the Late Devonian to Early Carboniferous. Both elemental abundances of carbon, nitrogen, and sulfur, along with concentration of trace metal and their analysis will be examined.

The core samples were retrieved November 5th, 2020. Each sample is labeled as RSM standing for the Riddlesburg Shale Member, and the associated depth in feet. To date all the RSM core samples have been crushed, grinded into a powder and acidified. The residues have all been analyzed for carbonate abundance and elemental analysis. The most important precaution that was considered was to ensure the samples would not be contaminated by metals. The metal tools used to crush the samples into smaller, pea-sized fragments, were wrapped several times over in cellophane. This included an iron weight and a chisel point Estwing rock hammer. The weight was placed on top of cardboard and fabric, then wrapped in the cellophane. Weighing paper was placed on top of the wrapped iron weight, and the samples that were being crushed were also wrapped in the cellophane. Most of the RSM samples had silty stringers and pockets of silt to fine grained sand particles within their matrix. The shale intervals were of interest for analysis; therefore, each sample was struck to separate the shale from the silt and sand of the

samples. Both tools were re-wrapped after each strike to the sample if a tear formed through a layer of the cellophane, this occurred after every strike.

Once each sample was crushed into pea-sized clasts they were ready to be grinded in a non-metal environment. This was facilitated by dispensing the clasts into an agate ball mill; the mill was filled to a third of its capacity then taped to secure it during the grinding. The jar consisted of a two agate caps, two malleable washers, and an agate cylinder. After being tapped the jar was secured inside of the 8000M Mixer/Mill. This device is a high energy ball that vigorously shakes the jar, combining back-and-forth swings with lateral movements; the clamped jar experiences strong G-forces inside, and the materials are pulverized. After the several minutes inside of the 8000M Mixer/Mill most of the clasts were rendered into a powder, the rounded pieces left was small and usually ranged from 3 to 6 mm in diameter. The inside of the agate jar was cleaned after a sample was grinded, once with ethanol and a second time with quartz sand. The first cleaning was performed by taking a kimwipe and cleaning the inside of the jar's components by hand with ethanol. Afterwards, the jar was loaded with pure quartz sand and clamped back into the 8000M Mixer/Mill to scrap out finer particles and organic material stuck on the inside of the jar. A third cleaning with kimwipes and ethanol was completed before loading a different RSM sample into the jar. The powders that were yielded from this grinding of the RSM samples were poured into 50 mL centrifuge vials to be acidified later.

Acidification of powders

Carbonates within the powders were acidified and decanted out before analysis in Elemental Analyzer/Isotope Ratio Mass Spectrometry (EA-IRMS) and Inductively Coupled Plasma Mass Spectrometry (ICP-MS). For the acidification process an approximate one-gram portion of each RSM sample placed into an additional centrifuge vial and labeled with the empty weight of that centrifuge vial, the weight of the sample to be acidified, and the corresponding RSM bulk sample. 3M HCl was administered to each vial up to the 10 mL line. The vials were then mixed on top of the Vortex Genie 2 and left under a fume hood overnight. The following day the solutions were spun and the supernatant was poured out of each tube prior to being treated with hot 3M HCl. The HCl was heated on a VWR VMS-C10 hot plate to a temperature of 125° Celsius. Like the first treatment, each vial received now hot HCl to the 10 mL line. The vials were mixed again in the Vortex Genie 2 but were left to settle for one hour instead of overnight. Each vial was loaded into the IEC Centra MP4 centrifuge and spun at 3800 rpm for eight minutes. Allowing the centrifuge to spin the vials stratified the particles from the supernatant and enabled the supernatant to be poured out of the vials . 18 MΩ Milli-Q water was added to the vials up to the 25 mL line and mixed with the residue, centrifuged, and then decanted. This was done four times to neutralize any remaining HCl in the solutions.

Elemental Analyzer (EA)

Prior to isotope analysis the vials were dried at 80°C overnight in the Valtech Economical Oven. The stratified contents of the centrifuge vials were homogenized with a glass stirring rod. Three repetitions of the RSM sample being analyzed were used to measure the total sulfur and $\delta^{33/34}S$ abundances. Both were measured by adding 19.0-23.0 mg aliquots of the acidified powder into tin cups. 200 μg of vanadium pentoxide (V_2O_5) was also added with the powder; V_2O_5 was added for the increase to oxidation efficiency it provides during combustion of the sample. Samples were placed within the sample carousel, the first sample dropped directly

into the combustion column filled with helium. The sulfur dioxide (SO_2) produced from combustion was transported into the gas chromatography column by the flow of helium being pumped into the system. The SO2 is purified in the column so that it comes out as a discrete peak. The gas then enters the source of the mass spectrometer where it is bombarded by electrons boiled off a thoria coated filament. The electrons knock electrons off the SO2 molecule, thus forming a positive SO2+ ion. There is a 3kV potential difference between the source and the cups, so the ions flow towards the negatively charged cups. As they travel, they are separated by the electromagnet based on their masses that then impact on five different cups (m/z 64, 66, 48, 49, and 50). Carbon samples were measured in ~1 gram aliquots and nitrogen samples were measured in ~20 gram aliquots.

Standards

The S analyses in the study were compared to the 0.1 mg aliquots of the NIST standard for barium sulfate ($BaSO_4$), noted as NBS-127. The RSM samples were also compared with the LECO-062 standard for sulfur in soils and is more related to the RSM samples in terms of urea than the NBS-127.

Presentation of Data

Sample	Depth (ft)	Mass (g)	Thickness (in)	Observations
RSM-544.5	544.5		0.75	50% a dark, fissile shale. The other 50% is a siltier to very fine grain sandy shale.
RSM-545.0	545.0	43.7	0.5	Fissile black shale.
RSM-548.0	548.0	72.9	1	Siltier black shale with laminations.
RSM-548.5	548.5	57.6	0.5	Five distinct layers of fissile black shale and siltier shale present.
RSM-549.0	549.0	31.9	0.1	Fragmented pieces of fissile black shale.
RSM-550.0	550.0	42.6	0.625	80% shale, 20% silt. Silt bedded between 0.5 in. of shale and a thinner 0.0625 in. layer of shale.
RSM-551.0	551.0	36.8	0.75	Black, fissile shale. Several silt/fine grained sand stringers visible in matrix.
RSM-552.0	552.0	25.6	0.5	66% of sample is black shale, 33% is silt. Sample displays laminations, stringers and pockets of siltier particles within the shale portions. Two concretions present in silt layer.
RSM-553.5	553.5	87.7	1	Black, fissile shale. Several silt/fine grained sand stringers visible in matrix.
RSM-554.5	554.5	57.7	0.875	Black shale with silt stringers appearing for a 0.25 in. interval. Pockets of silt and possible concretions also present in the sample. Small pockets of pyrite also visible.
RSM-555.0	555.0	66.4	1.25	Wavy bedding, crossbedding, pockets of sand sized particles are present with pockets of pyrite.
RSM-556.0	556.0	65.1	1	Black shale silt stringers and pockets of silt to very fine-grained sand particles.

RSM-557.0	557.0	58.1	0.625	Mostly siltier material, about 25% is shale. Silty layers are laminated.
RSM-557.5	557.5	72.6	1	Black shale with silt stringers, left side of sample has a bit of pyrite and a pocket of reddish brown, oxidized material.
RSM-558.5	558.5	70.6	1	Dark gray silty shale with trough crossbedding.
RSM-559.5	559.5	31.4	0.5	Laminated silt and shale
RSM-560.5	560.5	40.6	0.875	Light gray shale with silt strings. Silt strings are discontinuous around a pocket of silty particles or a possible concretion.
RSM-561.5	561.5	33.1	0.6875	Black, fissile shale. Several silt/fine grained sand stringers visible in matrix.
RSM-562.5	562.5	42.9	0.5	Black, fissile shale. Crossbedding is faintly visible.
RSM-563.2	563.2	54.3	1.25	Black shale with laminations, two small pockets of pyrite and small pockets of silt sized particles visible.
RSM-564.0	564.0	46	0.625	Black, fissile shale. One pocket of very fine-grained sand in matrix, Two smaller pockets of pyrite also in matrix.
RSM-565.0	565.0	59.6	0.75	Black, fissile shale. Dark pocket is a possible concretion or plant material.
RSM-566.0	566.0	52.7	0.5	Mostly silt
RSM-567.0	567.0	36.6	0.8125	Black, fissile shale with several silty stringers. Small pockets of pyrite.
RSM-568.0	568.0	76.6		
RSM-569.3	569.3	51.7	1.125	66% black shale, 33% silt to fine grained sand. Pockets of fine-grained sand inside of shale layers.
RSM-570.5	570.5	28.8	0.625	Black, fissile shale, laminations, flame cast structure is present.
RSM-571.5	571.5	59.7	1.5	Black shale with silt stringers and silt pockets.
RSM-572.5	572.5	22.7	0.625	Fragmented pieces of fissile black shale.
RSM-573.5	573.5	28	0.6875	Black, fissile shale with fine grained sand stringers.
RSM-575.0	575.0	33.7	0.25	Fragmented pieces of fissile black shale.
RSM-576.5	576.5	46.7	0.75	Black, fissile shale with two fine grained sand stringers.
RSM-577.5	577.5	37.7	0.875	Black, fissile shale. Laminated, flame cast, has a thin layer of sand.
RSM-578.5	578.5	68.9	0.9375	Black, fissile shale.
RSM-579.0	579.0	93.4	1.125	0.5 in. layer of very fine-grained sand particles.
RSM-580.7	580.7	27.7	0.5	Black, fissile shale. Sample is fragmented.
RSM-582.5	582.5	73.8	1	Black, fissile shale. Several sand stringer present.

Table 1. Sedimentological observations of all RSM cores retrieved from the PAGS

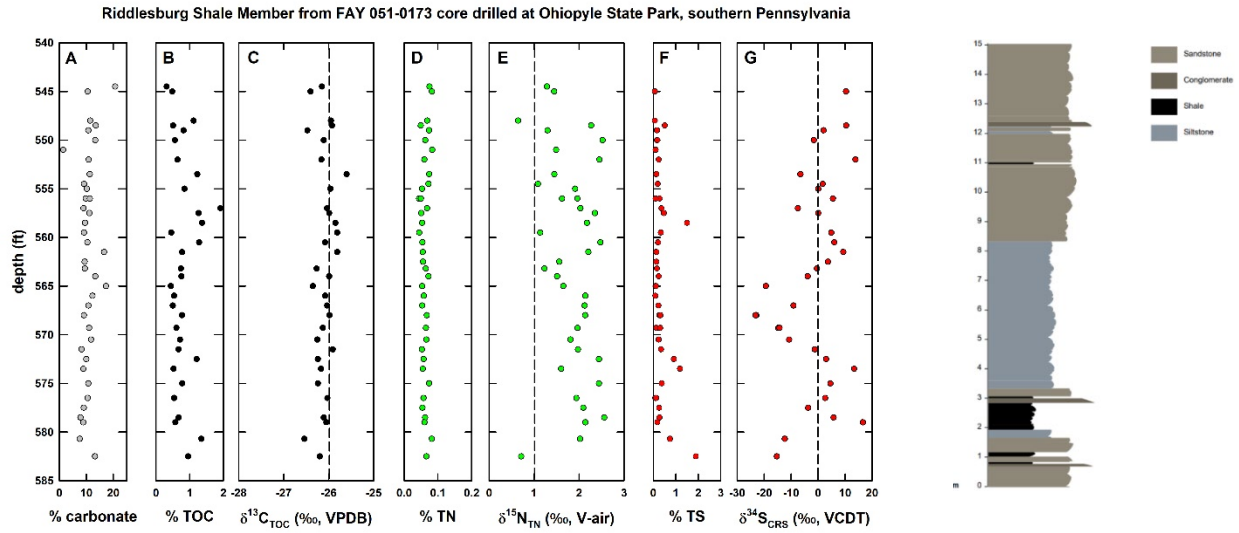

Figure 11. Time-series geochemical trends through the Riddlesburg Shale Member in the FAY 051-0173 core, including all 41 samples analyzed for the abundance of carbonate, TOC, total nitrogen (TN), and total sulfur (TS), as well as their carbon, nitrogen, and sulfur isotope analyses.

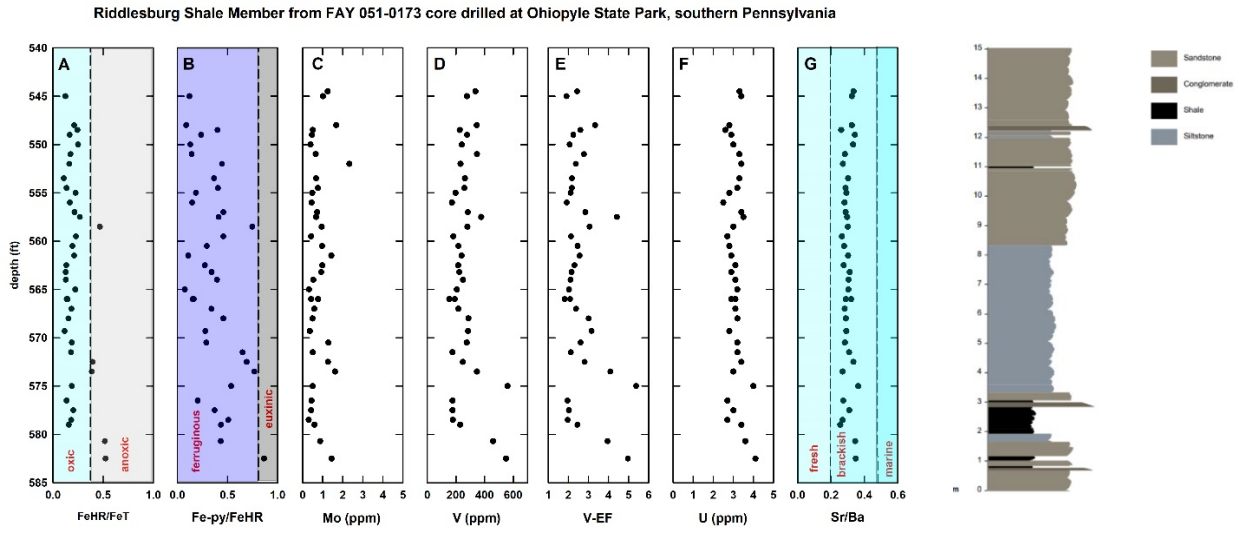

Figure 12. Time-series geochemical trends through the Riddlesburg Shale Member in the FAY 051-0173 core, including all 41 samples analyzed for the abundance of RSTMs (Mo, U, and V), paleosalinity (using the ratio of Sr to Ba), and paleoredox conditions of the Appalachian Basin during the deposition of the Riddlesburh Shale Member (RSM).

Discussion

Riddlesburg Shale Member lithology

The Riddlesburg shale possesses a coarser-grained lithology than the Bakken shale. This can be attributed to the differences both of their corresponding depositional environments received by means of tectonic activity. The Williston Basin did not receive such a large influx of continental material during the deposition of the Bakken shale. The heterolithic assemblage of the Riddlesburg shale is the product of the Acadian highlands slowly being eroded and deposited into the Appalachian Basin. The majority of RSM samples were a mixture of silt to very fine-grained sand particles and shale intervals comprised of clay sized particles. Within most shale intervals strings of the coarser particles were observable; some of these coarser particles formed larger pockets within the shale as well. In core samples RSM-569.3, RSM-570.5, and RSM-577.5 load casts are an observable sedimentary structure. The presence of these load casts is indicative of periods of denser loads being deposited on top of less dense layers of sediment. This would have been caused by the erosion of Acadian highland crustal rocks and their incorporation into the Appalachian Basin.

Percent carbonate

The average percentage of total carbonate species in the Riddlesburg is around 10% (Fig. 11A), this is half the amount found throughout the Bakken Formation (Fig. 9). It is important to understand the inventories of nutrients that were present in the Appalachian Basin compared to the Williston Basin. The low percentages of carbonate may be a product of the amount of biogeochemical activity present in the Appalachian Basin during the Devonian-Carboniferous transition. Based on the percent total organic carbon, total nitrogen, and total sulfur present in the Riddlesburg the Appalachian Basin is relatively deficient in nutrients sourced from the mixing and recycling of water. This is comparative to the Bakken Formation, bearing higher amounts of nutrients in the Williston Basin's reservoir. If microbial reduction was a source of alkalinity in the euxinic waters of the Williston Basin, then the less nutrient rich Appalachian Basin would show a trend of having less authigenic carbonate deposition.

Carbon (C)

The $\delta^{13}C_{TOC}$ fluctuate around -26‰ (Fig. 11B) and remain invariant moving up the stratigraphy. What is important here is the lack of any meaningful excursions present in the data. Stated earlier in the discussion of the Bakken data, organisms preferentially take the lighter ^{12}C isotope for their metabolic functions. The initial assumption made about the Riddlesburg in this study argued that the Appalachian Basin's proximity to the Acadian highlands meant moderate to enriched amounts of organic matter would find its way to the basin. Organisms have a $\delta^{13}C$ signature of around -25‰ (Racik, 2012), which in turn is very close to the RSM $\delta^{13}C$ -26‰ average. There seems to have been no significant changes to the enrichment of the Appalachian Basin with organic carbon, despite its proximity to the terrestrial environment.

Nitrogen (N)

RSM $\delta^{15}N_{TN}$ (Fig. 11E) trends behave in a similar oscillating fashion that is observed in the UBS. However, the Appalachian Basin has a terrestrial source of organic matter in the form

of land plants. The RSM data for $\delta^{15}N_{TN}$ is consistently positive and above 0‰, ranging from near 0‰ to <+3‰. The less positive intervals recorded are still assumed to be downtime in the primary productivity of denitrifiers in the Appalachian Basin. The increasingly positive trend is a product of N^{15} being sourced to the basin with the microbial community readily using nitrate as their electron acceptor. The LB1, 2, and 3 (Fig. 9) units of the Bakken show trends of anoxic expansions in terms of its $\delta^{15}N$ values while the RSM $\delta^{15}N_{TN}$ trend closer to zero up the stratigraphy and represent an "oxic" expansion. The redox conditions of the Appalachian Basin during deposition of the RSM (Fig. 11A) show that the basin became increasingly oxic as deposition continued, hence the description of the $\delta^{15}N_{TN}$ describing an oxic expansion seems to be in agreement with the redox conditions.

Sulfur (S)

The sulfur concentration in the residues was so low (Fig. 11F), however, that these analyses were suspect, and a decision was made to extract sulfur from all the bulk powders using a modified Chrome Reducing Solution (CRS) to reduce the pyrite in the acidified residues to H_2S gas that was passed through a $AgNO_3$ solution to form a purified Ag_2S precipitate. This work was performed by Prof. Kaufman, and after cleanup and drying, the Ag_2S precipitates were gravimetrically quantified, crushed, and aliquots weighed with an oxidant (V_2O_5) for mass spectrometric analysis. $\delta^{34}S$ of RSM samples reveal a large 50‰ shift in the in the stratigraphy, oscillating from -30‰ to nearly +20‰. Yes, there was sulfate reduction occurring in the Appalachian Basin but the question of how this sulfate is being sourced to the basin is present. Drastic shifts in the availability of sulfate could be the product of the basin's geography. The mass wasting of continental material rich in sulfates is a strong likelihood, a large depositional event, or sequential depositional events of continental crust enriched in sulfates would also have a potential effect of the sequestering of trace metals from the water column into the sediment.

Redox conditions of the Appalachian Basin

Iron speciation data for the base of the RSM suggests momentary anoxia (Fe_{HR}/Fe_T ~0.5) below the 580ft depth (Fig 12A). Above 580ft the bottom waters of the Appalachian Basin are definitively oxic (Fe_{HR}/Fe_T <0.38) based on the iron speciation data. Exceptions to this are the 572.5 and 573.5 ft depths which are ambiguous, along with the 558.5 ft anoxic data point. The Fe_{py}/Fe_{HR} ratio for the 582.5ft depth point (Fig. 12B) is the only record of euxinic conditions being present in the Appalachian Basin. Above this depth no record of euxinic conditions exist and a shift towards increased ferruginous conditions is present. These data suggest that the Appalachian Basin was dominated by relatively oxic waters; any anaerobic processes were restricted to the sediment.

Molybdenum (Mo) and Uranium (U)

Molybdenum concentrations in the RSM (Fig. 12C) are two and sometimes three orders of magnitude lower than what is observed in the Bakken units (Fig. 10). This should be expected when considering the basin was very oxic and only spent a brief period under euxinic conditions. Mo is transferred to sediment differently under oxic conditions comparatively to a reducing setting. Under oxic conditions, Mo is scavenged by metal oxides such as Mn, and further

speciated from molybdate oxyanion (MoO_4^{2-}) to the particle reactive molybdite (MoO_3) (Algeo & Tribovillard, 2009).

The RSM is more enriched in U than Mo, unlike the Bakken (Fig. 10). Under oxic–suboxic conditions, U is present mainly as soluble U(VI) in the form of uranyl carbonate complexes ($UO_2(CO_3)_3^{4-}$) that are chemically unreactive (Langmuir, 1978; Klinkhammer & Palmer, 1991; Calvert & Pedersen, 1993; Algeo & Tribovillard, 2009). U_{auth} enrichment is limited in oxic environments, and modern continent-margin sediments typically contain only 1–5 ppm (Morford et al., 2009b; Algeo & Tribovillard, 2009). Concentrations around 4 ppm are observed in the RSM but normalize around 3 ppm moving up the stratigraphy.

Vanadium (V) and Vanadium Enrichment Factor (V-EF)

The base of the RSM is moderately enriched in V at concentrations of 400-600 ppm at some points below the 575ft depth. These concentrations are like the ones observed in LB2 and LB3 prior to the maximum transgression of euxinic waters (Fig. 10). The bottom waters of the Appalachian Basin were less oxic and initially anoxic at the start of the RSM's deposition. The reduction of vanadate to lower oxidation states (vanadyl or V^{3+}), which are then retained in the sediment (Shiller & Mao, 1999; Gustafsson, 2019) seemed to have occurred readily in at the base of the RSM, near 600 ppm. The adsorption of vanadate to sedimentary iron oxides can also help to bind vanadium into the sediment (Auger et al., 1999, Gustafsson, 2019). The 200 ppm average for V, observed moving up the RSM stratigraphy (Fig. 12D), is congruent with the necessary Fe conditions found in the Appalachian Basin during the deposition of the RSM.

The RSM also displayed an enrichment factor in V at 3 to 5 times the amount present in Rockwell Formation, therefore 3 to 5 times more enriched than the continent. It is very possible that Late Devonian-Early Carboniferous seawater was enriched in V and was then sequestered into the soil by redox interactions with Fe, and organic matter.

Mo/U sequestration: oxic vs anoxic conditions

Redox conditions of the Appalachian Basin have been assessed through iron speciation of the RSM core bulk powders (Fig. 12A, Fig 12B). The redox conditions of the Late Devonian Appalachian Basin were abundantly more oxic than what was presented in the Williston Basin (see Fig. 6). The Appalachian and Williston Basin paleoenvironments present a different condition in which RSTMs are transferred to the sediment via different pathways. Under oxic conditions, Mo is present in seawater as the stable and largely unreactive molybdate oxyanion (MoO_4^{2-}) (Algeo & Tribovillard, 2009). Mo_{auth} enrichment is limited in oxic environments, and modern continent-margin sediments typically contain only 1–5 ppm (Zheng et al., 2000; Morford et al., 2009a; Algeo and Tribovillard, 2009). Mo abundance in the RSM core data never exceeds 3 ppm, and at some depths severely unabundant (<0.3 ppm) (Fig. 12C).

Under anoxic–sulfidic conditions (such as in the Williston Basin, see Fig 9), Mo becomes "activated" at a critical activity of hydrogen sulfide ($a_{HS^-} = 10^{-3.6}$ to $10^{-4.3}$, equivalent to ~ 50–250 μM HS^-), which facilitates conversion of molybdate (MoO_4^{2-}) to thiomolybdates ($MoO_xS_{(4-x)}^{2-}$, x = 0 to 3) (Helz et al., 1996; Zheng et al., 2000; Algeo & Tribovillard, 2009).

Although uptake of Mo by particulates can occur within the water column, under very euxinic conditions (Fig. 10 LB3, where a maximum transgression of euxinic waters occurs), most Mo uptake probably occurs at or just below the sediment/water interface (François, 1988, Emerson & Huested, 1991; Crusius et al., 1996; Zheng et al., 2000; Morford et al., 2009a; Algeo & Tribovillard, 2009). Mo transferred to sediment may be due to the much longer residence time of particles on the seafloor than in the water column, or possibly due to the higher sulfide concentrations encountered below the sediment/water interface (Meyers et al., 2005, Algeo & Tribovillard, 2009). Other factors that may favor Mo uptake at or below the sediment/water interface include the presence of Brønsted acids in porewaters, which promote the molybdate-to-thiomolybdate conversion, and the availability of clay mineral surfaces, which may catalyze hydrolysis and sulfidation of thiomolybdates (Erickson & Helz, 2000; Vorlicek & Helz, 2002; Algeo & Tribovillard, 2009). The hyper-enrichment of Mo in the LB3 and UB2, and the moderate enrichment throughout the Bakken shale suggests these conditions were present in the Williston Basin. Low Mo observed in the Appalachian Basin suggests Mo uptake was limited to occurring below the sediment/water interface, after the brief period of euxinic conditions recorded below the 580 ft RSM depth. This assertion may also be supported by the trend in U abundance present in the RSM cores.

Under oxic–suboxic conditions (RSM core iron speciation data, Fig. 12A and Fig. 12B) U is present mainly as soluble U(VI) in the form of uranyl carbonate complexes ($UO_2(CO_3)_3^{4-}$) that are chemically unreactive (Langmuir, 1978; Klinkhammer & Palmer, 1991; Calvert & Pedersen, 1993; Algeo & Tribovillard, 2009). U_{auth} enrichment is limited in oxic environments, and modern continent-margin sediments typically contain only 1–5 ppm (Morford et al., 2009b; Algeo & Tribovillard, 2009). This is congruent with the RSM uranium abundance never exceeding 4 ppm. Under anoxic conditions, like what is observed in the Bakken, U(VI) is reduced to U(IV), forming the highly soluble uranyl ion UO_2^+ or less soluble uranous fluoride complexes (Algeo & Tribovillard, 2009). U(VI) reduction would have taken place not only on particle surfaces, possibly catalyzed by enzymes produced by iron and sulfate-reducing bacteria (Barnes and Cochran, 1990; Zheng et al., 2002a; Morford et al., 2009a; Algeo & Tribovillard, 2009), but also in the water column to some degree in the Williston Basin. Uranium sequestering to sediments can occur by means of: (1) formation of organic-metal ligands in humic acids, or (2) precipitation of crystalline uraninite (UO_2) or a metastable precursor to it (Klinkhammer & Palmer, 1991; Zheng et al., 2002a; Algeo & Tribovillard, 2009). U reduction also commences at the Fe(II)–Fe(III) redox boundary and may be controlled by microbially-mediated Fe redox reactions rather than by the presence of HS^- (Zheng et al., 2002a; Algeo & Tribovillard, 2009). In turn, this would mean that the ferruginous conditions of the Appalachian Basin bottom waters were more suitable for the sequestering of U over Mo. This is supported by the observations on the onset of U_{auth} enrichment occurs under less intensely reducing conditions and at shallower depths within the sediment column than that of Mo_{auth} (Morford et al., 2009a; Algeo & Tribovillard, 2009).

Conclusions

Geochemical data for both the Bakken and Riddlesburg shale have preserved a record of the redox conditions of the basins and the activity of the anaerobic microbes residing with the

sediment. The glacial mobilization of nutrients (C_{TOC} and N_{TN}), reductants (SO_4^{2-}), and RSTMs (Mo, U, and V), like in other shales, activated the microbial communities at the sediment-water interface.

Hypotheses

3. The glacial mobilization of nutrients, sulfate, alkalinity, and trace metals from the Acadian highlands into the Appalachian foreland basin affected biogeochemical processes and spurred anoxic and potentially euxinic (free H_2S in the water column) conditions across the Devonian-Carboniferous transition.
4. Changes to redox conditions affected the sequestering of redox sensitive trace metals (RSTMs) in the organic rich foreland Appalachian Basin sediments.

Based on the RSM core data regarding elemental analyses (Fig. 11) and redox conditions and trace metal abundance (Fig. 12), (1) should be rejected. While euxinic conditions are briefly observed in the Appalachian Basin based on the RSM core data, these conditions were not long lasting. Anoxia was only definitively present below the 580 ft depth the stratigraphy, correlating to whenever that may be during the deposition of the RSM in the Appalachian Basin. Above this depth the RSM cores record more oxic conditions. The Appalachian Basin was mostly oxic during the Devonian Carboniferous transition.

(2) should be accept, insofar that redox conditions of the Appalachian Basin did become progressively more oxic, affecting RSTM concentrations. Notably, it is the change from anoxic to oxic, and euxinic to ferruginous where a significant effect on the sequestration of RSTMs to the sediment occurred in Appalachian Basin. RSTM enrichment in the Riddlesburg was 2 and sometimes 3 orders of magnitude less than what was observed in the Bakken Shale units. No Mo/V anti-correlation is present in the Riddlesburg Shale Member core data, but U is proportionally more abundant in the Riddlesburg Shale Member than in the Bakken Shales.

Moving up the RSM stratigraphy, U abundance drops from <5 ppm to 3> ppm (Fig. 12F). The lower U abundance correlates positively with increased oxic conditions (Fig. 12A). It is plausible that increased oxic conditions were welcoming to biota, increasing bioturbation is potentially releasing U back into the water column. There, U would either have been carried out of the Appalachian Basin during a water mixing event or re-sequestered back into the sediment. Mo and V trends (Fig. 12C and Fig. 12D) may be related to the %TOC that was available in the Appalachian Basin (Fig. 11B). A similar trend in %TOC and RSTM enrichment is present in the Bakken Shale data as well (Fig. 9 and Fig. 10).

The lower overall nutrient in the Riddlesburg Shale Member (Fig. 11) directly affected the ability for microbial communities to reduce redox sensitive elements and create anoxic conditions. Anaerobic processes were restricted at and below the sediment-water interface, and the euxinic conditions that were present in the Williston Basin were not present in the Appalachian Basin during the Devonian-Carboniferous transition. Vanadium is the only RSTM of the three involved in this study that showed enrichment similar to the Bakken Shales.

Future Work

Sunbury Shale

The Sunbury Shale is an equivalent shale further to the west and south in the Appalachian Basin. Gilleaudeau (2021) performed a similar study on 5 cores through the Sunbury Shale from northeastern Ohio to southern Kentucky. The Sunbury Shale in one of the cores analyzed is a grey shale with low TOC and evidence for transport of coarser-grained material to the area. Like the Riddlesburg Shale, the iron speciation is oxic to equivocal, Mo is not enriched, and V is enriched similarly to the Riddlesburg. The Sr/Ba ratio for the Sunbury also shows low-brackish conditions which also align with what has been observed in the Riddlesburg Shale Member. For future research, the Sunbury will be compared to the Riddlesburg Shale Member to better understand the Devonian-Carboniferous transitional Appalachian Basin conditions. The enrichment factors of Mo and U will also be compared to what is present in the Sunbury.

Figure 13. Paleogeographic map of North America during the Late Devonian to Early Mississippian (map originally generated by R. Blakey) with inset showing specific locations of the five study cores in Ohio and Kentucky. Paleogeography modified from Algeo et al. (2007)and inset constructed using Google Earth. (Gilleaudeau, 2021)

Acknowledgements

I want to thank both of my advisors on this project, Dr. Jay Kaufman and Dr. Geoffrey Gilleaudeau for their support and guidance through the project, as well as their assistance in the creation of figures used. I am also thankful for their motivation and insight into the nature of this study on the Riddlesburg Shale Member. I am also greatly appreciative towards John Neubaum for helping in the retrieval of them RSM core samples and prior for the assistance in pinpoint where the Riddlesburg outcrops in Pennsylvania. I thank Cristy Ho as Lab Manager, Richard Ash for the use of his lab, Richard Walker and Phil Piccoli for support from the Stifel Fund for the project, and Allie Boyle for assistance in core sampling.

"I pledge on my honor that I have not given or received any unauthorized assistance or plagiarized on this assignment."

Justus McMillan

Appendix

sample	depth (ft)	carbonate (%)	TOC (%)	d13C	%N	d15N	%S	d34S
RSM-544.5	544.5	20.71238807	0.31715045	-26.15	0.07	1.29		
RSM-545.0	545	10.51983714	0.48458476	-26.4044	0.08	1.45		
RSM-548.0	548	11.42203449	1.11608237	-25.95	0.07	0.65		
RSM-548.5	548.5	13.51724138	0.50608804	-25.9247	0.05	2.27		
RSM-549.0	549	10.74332172	0.81760069	-26.4733	0.07	1.30		
RSM-550.0	550	13.30161562	0.56254951	-26.1097	0.07	2.52		
RSM-551.0	551	1.432189328			0.08	1.49		
RSM-552.0	552	10.852135	0.64186463	-26.16	0.06	2.45	11.83	13.86
RSM-553.5	553.5	11.27819549	1.2243609	-25.6	0.07	1.45		
RSM-554.5	554.5	9.160984287			0.07	1.09	12.76	1.72
RSM-555.0	555	10.19743147	0.84414414	-25.96	0.05	1.92	12.29	0.05
RSM-556.0A	556	9.796655264			0.04	1.62		
RSM-556.0B	556	11.31728826			0.05	1.97		
RSM-557.0	557	8.916433427	1.9127549	-26.04	0.07	2.03		
RSM-557.5	557.5	11.1368084	1.26185732	-25.99	0.05	2.35	13.18	13.18
RSM-558.5	558.5	9.513876292	1.36634047	-25.85	0.05	2.18	12.87	12.87
RSM-559.5	559.5	9.174889775	0.45412555	-25.81	0.04	1.14	12.03	12.03
RSM-560.5	560.5	10.40221914	1.28124827	-26.08	0.05	2.48		
RSM-561.5	561.5	16.59491194	0.77566732	-25.81	0.05	2.21		
RSM-562.5	562.5	9.388700472			0.06	1.56		
RSM-563.2	563.2	9.453369906	0.74248237	-26.27	0.06	1.23	13.01	13.01

RSM-564.0	564	13.34945169	0.75385977	-25.99	0.07	1.51	11.3	11.3
RSM-565.0	565	17.29645501	0.44284007	-26.3525	0.05	1.65		
RSM-566.0	566	12.29606049	0.53499403	-26.08	0.06	2.14		
RSM-567.0	567	10.77175065	0.49815566	-26.0344	0.05	2.13	12.95	12.95
RSM-568.0	568	9.110898662	0.77386059	-25.9832	0.07	2.14	12.14	12.14
							12.83	12.83
RSM-569.3	569.3	11.02955763	0.60687286	-26.1302	0.06	1.97	6.65	6.65
							12.78	12.78
RSM-570.5	570.5	11.73211989	0.7128178	-26.2516	0.07	1.81	10.9	10.9
RSM-571.5	571.5	8.229665072	0.66992344	-25.91	0.05	1.98	12.93	12.93
RSM-572.5	572.5	9.998122418	1.20602516	-26.24	0.06	2.44	13.48	13.48
RSM-573.5	573.5	8.909494054	0.51921588	-26.17	0.05	1.60	12.25	12.25
RSM-575.0	575	10.74642668	0.77650609	-26.24	0.07	2.44	12.76	12.76
RSM-576.5	576.5	10.49124901	0.53705251	-26.03	0.06	1.94	12.5	12.5
RSM-577.5	577.5	9.071167703			0.05	2.10	12.99	12.99
RSM-578.5	578.5	7.83310372	0.67281834	-26.11	0.06	2.56	12.73	12.73
RSM-579.0	579	8.832425892	0.57435572	-26.05	0.06	2.14	12.84	12.84
RSM-580.7	580.7	7.530423644	1.34710144	-26.5396	0.08	2.02	13.78	13.78
RSM-582.5	582.5	13.21329158	0.95465379	-26.2	0.07	0.71	13.09	13.09

Table 2. Elemental analysis of all RSM cores retrieved from the PAGS

Sample	Type	Mo	V	U	Mn	Ba	Sr
LB1-2-3-95	Shale	186.64	316	49.9	63	135	52
LB1-2-4-29	Shale	295.93	422	57.3	86	217	59
LB1-2-4-69	Shale	306.65	231	47.4	91	190	59
LB1-2-5-45	Shale	250.1	235	66.6	113	254	77
LB1-2-5-5	Shale	212.77	223	54.8	100	212	66
LB1-2-5-9	Shale	234.43	222	80.5	116	226	91
LB1-2-5-90	Shale	258.1	227	75.3	126	206	79
LB1-2-6-28	Shale	183.32	243	46.8	116	363	70
LB1-2-6-55	Shale	29.89	193	26.4	136	292	82
LB1-2-6-75	Shale	119.4	177	37.1	160	171	89
LB1-2-7-16	Shale	1.72	110	2.5	141	327	78
LB1-2-7-84	Shale	0.59	86	1.8	547	281	126
RSM-544.5	Shale	1.25	337	3.3	1047	663	222
RSM-545	Shale	1.01	277	3.4	420	653	212
RSM-548	Shale	1.67	345	2.8	365	493	160
RSM-548.5	Shale	0.51	227	2.6	122	437	114
RSM-549	Shale	0.46	278	2.9	458	502	172
RSM-550	Shale	0.39	241	3	673	545	181
RSM-551	Shale	0.65	347	3.3	561	611	173
RSM-552	Shale	2.33	232	3.4	242	516	140
RSM-553.5	Shale	0.67	263	3.3	193	576	174
RSM-554.5	Shale	0.76	259	3.2	176	599	172
RSM-555	Shale	0.48	197	2.8	249	486	142
RSM-556B	Shale	0.45	172	2.5	304	456	128
RSM-557	Shale	0.72	283	3.4	294	542	156
RSM-557.5	Shale	0.67	377	3.5	363	475	141
RSM-558.5	Shale	0.95	280	3	140	499	150
RSM-559.5	Shale	0.42	181	2.7	138	440	117
RSM-560.5	Shale	0.97	217	2.8	334	474	132
RSM-561.5	Shale	1.43	240	2.9	843	480	145
RSM-562.5	Shale	0.98	216	3.1	264	515	142
RSM-563.2	Shale	0.93	223	2.9	167	490	153
RSM-564	Shale	0.53	250	3.1	363	599	183
RSM-565	Shale	0.32	206	3.2	698	535	163
RSM-566	Shale	0.42	192	2.9	288	526	152
RSM-566A	Shale	0.77	154	3.1	266	383	123
RSM-567	Shale	0.58	217	3.1	199	493	139
RSM-568	Shale	0.49	287	3.2	169	478	138
RSM-569.3	Shale	0.36	285	2.8	222	439	128

RSM-570.5	Shale	1.28	276	3.2	645	484	137
RSM-571.5	Shale	0.51	176	3.2	94	412	127
RSM-572.5	Shale	1.26	249	3.4	164	461	154
RSM-573.5	Shale	1.61	347	3	140	426	115
RSM-575	Shale	0.5	560	4	163	493	179
RSM-576.5	Shale	0.44	176	2.7	153	467	128
RSM-577.5	Shale	0.42	176	3	184	442	137
RSM-578.5	Shale	0.3	178	2.7	100	468	126
RSM-579.0	Shale	0.59	230	3.4	137	497	127
RSM-580.7	Shale	0.87	460	3.6	116	583	201
RSM-582.5	Shale	1.44	550	4.1	362	519	181
Rockwell Diamictite Matrix	Shale	0.61	63	4.7	1217	234	56

Table 3. Abundance of Mo, V, U, Mn, Ba, and Sr present in the LB1, RSM, and Rockwell diamictite matrix.

Iron speciation

Iron speciation analyses were conducted at George Mason University following published methods (Poulton and Canfield, 2005). Pyrite iron (Fe_{py}) was calculated (assuming a stoichiometry of FeS_2) from the mass of Ag_2S precipitated during a two-hour hot chromous chloride distillation (Canfield et al., 1986). Other iron species—specifically, Fe_{carb}, Fe_{ox}, 2 and Fe_{mag}—were extracted sequentially (Poulton and Canfield, 2005) using sodium acetate solution, dithionite solution, and ammonium oxalate solution, respectively. The ammonium oxalate solution has also been shown to extract iron-rich clay minerals (Slotznick et al., 2020). The sequential extracts were analyzed with an Agilent 7500ce inductively-coupled plasma mass spectrometer (ICP-MS). Total iron concentrations (FeT) is determined by HF-HNO3-HCl acid digestion followed by ICP-MS analysis. (Gilleaudeau, 2021)

Paleosalinity proxy (Sr/Ba)

Paleosalinity is examined in this study using the newly developed Sr/Ba proxy applied to carbonate-free, fine-grained siliciclastic sediments (Wei and Algeo, 2020; Remírez and Algeo, 2020; Song et al., 2021). Whereas freshwater exhibits low but variable Sr concentrations, seawater is strongly enriched in Sr (De Villiers, 1999). Strontium also has a long residence time in the modern ocean (2 to 5 Myr), meaning that its concentration is well-mixed across the global oceans (De Villiers, 1999). By contrast, Ba concentrations are higher in freshwater, and Ba is only found in trace amounts in seawater due to the low aqueous solubilities of typical Ba minerals (barite in particular in the presence of high seawater sulfate). The strong insolubility of barite suggests that variations in marine sulfate concentrations likely would not affect the Sr/Ba proxy, at least on the scale of sulfate variability thought to have occurred through the Phanerozoic Eon. Barium has a substantially shorter residence time than Sr (Ba residence time = ~8 kyr), although it is still longer than the ocean mixing time. Barium does exhibit a "nutrient-type" profile in the open ocean with lower concentrations in surface waters and higher concentrations in deep waters. This depth gradient would likely be less pronounced in shallow

intracratonic basins such as the Early Mississippian Appalachian Seaway, however. In general, the Sr/Ba proxy provides an integrated look at regional watermass chemistry. Through analysis of modern systems, Wei and Algeo (2020) suggested that Sr/Ba ratios less than 0.2 are indicative of freshwater, those between 0.2 and 0.5 suggest brackish conditions, and greater than 0.5 is indicative of marine conditions, although exact threshold values may be formation-specific. (Gilleaudeau, 2021)

Bibliography

Abarghani, A., Gentzis, T., Liu, B., Khatibi, S., Bubach, B., & Ostadhassan, M. (2020). Preliminary Investigation of the Effects of Thermal Maturity on Redox-Sensitive Trace Metal Concentration in the Bakken Source Rock, North Dakota, USA. *ACS Omega*, *5*(13), 7135–7148. https://doi.org/10.1021/acsomega.9b03467

Algeo, T. J., & Lyons, T. W. (2006). Mo-total organic carbon covariation in modern anoxic marine environments: Implications for analysis of paleoredox and paleohydrographic conditions. *Paleoceanography*, *21*(1), n/a. https://doi.org/10.1029/2004pa001112

Algeo, T. J., & Maynard, J. B. (2004). Trace-element behavior and redox facies in core shales of Upper Pennsylvanian Kansas-type cyclothems. *Chemical Geology*, *206*(3–4), 289–318. https://doi.org/10.1016/j.chemgeo.2003.12.009

Algeo, T. J., & Scheckler, S. E. (1998). Terrestrial-marine teleconnections in the Devonian: Links between the evolution of land plants, weathering processes, and marine anoxic events. *Philosophical Transactions of the Royal Society of London. Series B: Biological Sciences, 353*(1365), 113-130. doi:10.1098/rstb.1998.0195

Algeo, T., & Tribovillard, N. (2009). Environmental analysis of paleoceanographic systems based on molybdenum–uranium covariation. *Chemical Geology*, *268*(3–4), 211–225. https://doi.org/10.1016/j.chemgeo.2009.09.001

Auger, Y., Bodineau, L., Leclercq, S., & Wartel, M. (1999). Some aspects of vanadium and chromium chemistry in the English Channel. *Continental Shelf Research*, *19*(15–16), 2003–2018. https://doi.org/10.1016/s0278-4343(99)00050-3

Becker, B., & Marin, B. (2009). Streptophyte algae and the origin of embryophytes. *Annals of Botany*, *103*(7), 999–1004. https://doi.org/10.1093/aob/mcp044

Breit, G. N., & Wanty, R. B. (1991). Vanadium accumulation in carbonaceous rocks: A review of geochemical controls during deposition and diagenesis. *Chemical Geology*, *91*(2), 83–97. https://doi.org/10.1016/0009-2541(91)90083-4

Brennan. (2016, December 13). *Integrated characterization of middle Bakken diagenesis, Williston Basin, North Dakota, U.S.A.* Mountainscholar. https://mountainscholar.org/handle/11124/170243?show=full

Brezinski, D. K., Cecil, C. B., Skema, V. W., & Stamm, R. (2008). Late Devonian glacial deposits from the eastern United States signal an end of the mid-Paleozoic warm period. *Palaeogeography, Palaeoclimatology, Palaeoecology, 268*(3-4), 143-151. doi:10.1016/j.palaeo.2008.03.042

Calvert, S. E., & Pedersen, T. F. (1993). Geochemistry of Recent oxic and anoxic marine sediments: Implications for the geological record. *Marine Geology*, *113*(1–2), 67–88. https://doi.org/10.1016/0025-3227(93)90150-t

Calvert, S., & Pedersen, T. (1993). Geochemistry of Recent oxic and anoxic marine sediments: Implications for the geological record. *Marine Geology*, *113*(1–2), 67–88. https://doi.org/10.1016/0025-3227(93)90150-t

Caplan, M. L., & Bustin, R. (1999). Devonian–Carboniferous Hangenberg mass extinction event, widespread organic-rich mudrock and anoxia: Causes and consequences. *Palaeogeography, Palaeoclimatology, Palaeoecology, 148*(4), 187-207. doi:10.1016/s0031-0182(98)00218-1

Carmichael, S. K., Waters, J. A., Königshof, P., Suttner, T. J., & Kido, E. (2019). Paleogeography and paleoenvironments of the Late Devonian Kellwasser event: A review of its sedimentological and geochemical expression. *Global and Planetary Change, 183*, 102984. doi:10.1016/j.gloplacha.2019.102984

Chaloner, W. G., & Sheerin. (1979). THE RISE OF THE FIRST LAND PLANTS. *Biological Reviews*, *45*(3), 353–377. https://doi.org/10.1111/j.1469-185x.1970.tb01645.x

Christopher, J. E., 1961, Transitional Devonian-Mississippian Formation of Southern Saskatchewan. Regina, Saskatchewan, Canada, Saskatchewan Mineral Resources Geological Report 66, pp. 103.

Crusius, J., Calvert, S., Pedersen, T., & Sage, D. (1996). Rhenium and molybdenum enrichments in sediments as indicators of oxic, suboxic and sulfidic conditions of deposition. *Earth and Planetary Science Letters*, *145*(1–4), 65–78. https://doi.org/10.1016/s0012-821x(96)00204-x

Dahl, T. W., & Arens, S. K. (2020). The impacts of land plant evolution on Earth's climate and oxygenation state – An interdisciplinary review. *Chemical Geology, 547*, 119665. doi:10.1016/j.chemgeo.2020.119665

Dow, W. G., 1972, Application of oil correlation and source rock data to exploration in Williston basin (abs.): AAPG Bulletin, v. 56, p. 615.

Dow, W. G., 1974, Application of oil correlation and source rock data to exploration in Williston basin: AAPG Bulletin, v. 58, n. 7, p. 1253-1262.

Edwards, D., Davies, K. L., & Axe, L. (1992). A vascular conducting strand in the early land plant Cooksonia. *Nature, 357*(6380), 683-685. doi:10.1038/357683a0

Egenhoff, S. O., & Fishman, N. S. (2020). The Bakken Formation - understanding the sequence stratigraphic record of low-gradient sedimentary systems, shale depositional environments, and sea-level changes in an icehouse world. *The Sedimentary Record*, *18*(4), 4–9. https://doi.org/10.2110/sedred.2020.4.4

Emerson, S. R., & Huested, S. S. (1991). Ocean anoxia and the concentrations of molybdenum and vanadium in seawater. *Marine Chemistry*, *34*(3–4), 177–196. https://doi.org/10.1016/0304-4203(91)90002-e

Englund, W. (2020, March 13). *Oil companies say they plan to slash spending*. Dallas News. https://www.dallasnews.com/business/energy/2020/03/13/oil-companies-say-they-plan-to-slash-spending/

Erickson, B. E., & Helz, G. R. (2000). Molybdenum(VI) speciation in sulfidic waters: *Geochimica et Cosmochimica Acta*, *64*(7), 1149–1158. https://doi.org/10.1016/s0016-7037(99)00423-8

Erickson, B. E., & Helz, G. R. (2000). Molybdenum(VI) speciation in sulfidic waters: *Geochimica et Cosmochimica Acta*, *64*(7), 1149–1158. https://doi.org/10.1016/s0016-7037(99)00423-8

Faill, R. T. (1997). A geologic history of the north-central Appalachians; Part 2, The Appalachian Basin from the Silurian through the Carboniferous. *American Journal of Science, 297*(7), 729-761. doi:10.2475/ajs.297.7.729

Flint, R. F., Sanders, J. E., & Rodgers, J. (1960). Diamictite, A Substitute Term For Symmictite. *Geological Society of America Bulletin, 71*(12), 1809. doi:10.1130/0016-7606(1960)71[1809:dastfs]2.0.co;2

Frakes. (1992). *Climate Modes of the Phanerozoic*. Cambridge University Press. https://doi.org/10.1017/CBO9780511628948

François, L. M., & Gérard, J.-C. (1986). A numerical model of the evolution of ocean sulfate and sedimentary sulfur during the last 800 million years. *Geochimica et Cosmochimica Acta*, *50*(10), 2289–2302. https://doi.org/10.1016/0016-7037(86)90083-9

Fuex A. N. (1977) The use of stable carbon isotopes in hydrocarbon exploration. J. Geochem. Exploration. 7, 155-188.

Gaspar, J., Davis, D., Camacho, C., & Alvarez, P. J. J. (2016). Biogenic versus Thermogenic H2S Source Determination in Bakken Wells: Considerations for Biocide Application. *Environmental Science & Technology Letters*, *3*(4), 127–132. https://doi.org/10.1021/acs.estlett.6b00075

Gilleaudeau, G. J., Algeo, T. J., Lyons, T. W., Bates, S., & Anbar, A. D. (2021). Novel watermass reconstruction in the Early Mississippian Appalachian Seaway based on integrated proxy records of redox and salinity. *Earth and Planetary Science Letters*, *558*, 116746. https://doi.org/10.1016/j.epsl.2021.116746

Gillespie, W. H., Rothwell, G. W., & Scheckler, S. E. (1981). The earliest seeds. *Nature*, *293*(5832), 462–464. https://doi.org/10.1038/293462a0

Gustafsson, J. P. (2019). Vanadium geochemistry in the biogeosphere –speciation, solid-solution interactions, and ecotoxicity. *Applied Geochemistry*, *102*, 1–25. https://doi.org/10.1016/j.apgeochem.2018.12.027

Hart, B., & Hofmann, M. (2020). The Late Devonian Ice Age and the Giant Bakken Oil Field. *The Sedimentary Record*, *18*(1), 4–9. https://doi.org/10.2110/sedred.2020.1.4

Helz, G., Miller, C., Charnock, J., Mosselmans, J., Pattrick, R., Garner, C., & Vaughan, D. (1996). Mechanism of molybdenum removal from the sea and its concentration in black shales: EXAFS evidence. *Geochimica et Cosmochimica Acta*, *60*(19), 3631–3642. https://doi.org/10.1016/0016-7037(96)00195-0

Hoch, M. P., Fogel, M. L., & Kirchman, D. L. (1994). Isotope fractionation during ammonium uptake by marine microbial assemblages. *Geomicrobiology Journal*, *12*(2), 113–127. https://doi.org/10.1080/01490459409377977

Ketner, K. B. (2013). Stratigraphy of lower to middle Paleozoic rocks of northern Nevada and the Antler orogeny. *Professional Paper*. doi:10.3133/pp1799

Klinkhammer, G., & Palmer, M. (1991). Uranium in the oceans: Where it goes and why. *Geochimica et Cosmochimica Acta*, *55*(7), 1799–1806. https://doi.org/10.1016/0016-7037(91)90024-y

Knoll, A. H., Canfield, D. E., Konhauser, K. O., & Ward, B. (2012). *Fundamentals of Geobiology* (1st ed.). Wiley-Blackwell.

Korchef, A., & Touaibi, M. (2019). Effect of pH and temperature on calcium carbonate precipitation by CO 2 removal from iron-rich water. *Water and Environment Journal*, *34*(3), 331–341. https://doi.org/10.1111/wej.12467

Kunert, A., Clarke, J., & Kendall, B. (2020). Molybdenum Isotope Constraints on the Origin of Vanadium Hyper-Enrichments in Ediacaran–Phanerozoic Marine Mudrocks. *Minerals*, *10*(12), 1075. https://doi.org/10.3390/min10121075

Lang, W. H. (1937). IV - On the plant-remains from the Downtonian of England and Wales. *Philosophical Transactions of the Royal Society of London. Series B, Biological Sciences*, *227*(544), 245–291. https://doi.org/10.1098/rstb.1937.0004

Langmuir, D. (1978). Uranium solution-mineral equilibria at low temperatures with applications to sedimentary ore deposits. *Geochimica et Cosmochimica Acta*, *42*(6), 547–569. https://doi.org/10.1016/0016-7037(78)90001-7

Liu, J., Qie, W., Algeo, T. J., Yao, L., Huang, J., & Luo, G. (2016). Changes in marine nitrogen fixation and denitrification rates during the end-Devonian mass extinction. *Palaeogeography, Palaeoclimatology, Palaeoecology*, *448*, 195–206. https://doi.org/10.1016/j.palaeo.2015.10.022

Maldonado, D. N. (2014). Chemostratigraphy and Geochemical Constraints on the Deposition of the Bakken formation, Williston Basin, eastern Montana and western North Dakota.

Martinez, A. M., Boyer, D. L., Droser, M. L., Barrie, C., & Love, G. D. (2018). A stable and productive marine microbial community was sustained through the end-Devonian Hangenberg Crisis within the Cleveland Shale of the Appalachian Basin, United States. *Geobiology*, *17*(1), 27–42. https://doi.org/10.1111/gbi.12314

Milliman, J. D. (1993). Production and accumulation of calcium carbonate in the ocean: Budget of a nonsteady state. *Global Biogeochemical Cycles*, *7*(4), 927–957. https://doi.org/10.1029/93gb02524

Morford, J. L., Martin, W. R., & Carney, C. M. (2009). Uranium diagenesis in sediments underlying bottom waters with high oxygen content. *Geochimica et Cosmochimica Acta*, *73*(10), 2920–2937. https://doi.org/10.1016/j.gca.2009.02.014

Mosbrugger, V. (1990). V. Mosbrugger. The Tree Habit in Land Plants: a Functional Comparison of Trunk Constructions with a Brief Introduction into the Biomechanics of Trees. Springer-Verlag, Berlin 1990. pp 161 DM40,000. ISBN 3–540-52374-X. *Journal of Evolutionary Biology*, *4*(3), 516–517. https://doi.org/10.1046/j.1420-9101.1991.4030516.x

Nicas, J. (2016). Oil Fuels Population Boom in North Dakota City. *WSJ*. https://www.wsj.com/articles/SB10001424052702304072004577 3

Pawlik, Ł, Buma, B., Šamonil, P., Kvaček, J., Gałązka, A., Kohout, P., & Malik, I. (2020). Impact of trees and forests on the Devonian landscape and weathering processes with implications to the global Earth's system properties - A critical review. *Earth-Science Reviews, 205*, 103200. doi:10.1016/j.earscirev.2020.103200

R. H. Worden (2), P. C. Smalley (3). (1995). Gas Souring by Thermochemical Sulfate Reduction at 140øC. *AAPG Bulletin*, *79*, 1. https://doi.org/10.1306/8d2b1bce-171e-11d7-8645000102c1865d

R. H. Worden (2), P. C. Smalley (3). (1995). Gas Souring by Thermochemical Sulfate Reduction at 140øC. *AAPG Bulletin*, *79*, 1–5. https://doi.org/10.1306/8d2b1bce-171e-11d7-8645000102c1865d

Raiswell, R., & Canfield, D. E. (2012). The Iron Biogeochemical Cycle Past and Present. *Geochemical Perspectives, 1*(1), 1-220. doi:10.7185/geochempersp.1.1

Raven, J. A., & Edwards, D. (2001). Roots: Evolutionary origins and biogeochemical significance. *Journal of Experimental Botany, 52*(Suppl_1), 381-401. doi:10.1093/jxb/52.suppl_1.381

Römer, F. A. (1850). *Beiträge zur geologischen Kenntniss des nordwestlichen Harzgebirges / von Friedrich Adolph Römer. 1. - 5. Abtheilung*. Fischer. https://doi.org/10.24355/dbbs.084-201503171648-0

Rothwell, G. W., Scheckler, S. E., & Gillespie, W. H. (1989). Elkinsia gen. nov., a Late Devonian Gymnosperm with Cupulate Ovules. *Botanical Gazette*, *150*(2), 170–189. https://doi.org/10.1086/337763

Schobben, M., van de Schootbrugge, B., & Wignall, P. B. (2019). Interpreting the Carbon Isotope Record of Mass Extinctions. *Elements*, *15*(5), 331–337. https://doi.org/10.2138/gselements.15.5.331

Scott, C., Lyons, T. W., Bekker, A., Shen, Y., Poulton, S. W., Chu, X., & Anbar, A. D. (2008). Tracing the stepwise oxygenation of the Proterozoic ocean. *Nature*, *452*(7186), 456–459. https://doi.org/10.1038/nature06811

Scott, C., Slack, J. F., & Kelley, K. D. (2017). The hyper-enrichment of V and Zn in black shales of the Late Devonian-Early Mississippian Bakken Formation (USA). *Chemical Geology*, *452*, 24–33. https://doi.org/10.1016/j.chemgeo.2017.01.026

Sepkoski, J. J. (1979). A kinetic model of Phanerozoic taxonomic diversity II. Early Phanerozoic families and multiple equilibria. *Paleobiology*, *5*(3), 222–251. https://doi.org/10.1017/s0094837300006539

Shiller, A. M., & Mao, L. (1999). Dissolved vanadium on the Louisiana Shelf: effect of oxygen depletion. *Continental Shelf Research*, *19*(8), 1007–1020. https://doi.org/10.1016/s0278-4343(99)00005-9

Simon, L., Goddéris, Y., Werner Buggisch, Strauss, H., & Joachimski, M. M. (2007). Modeling the carbon and sulfur isotope compositions of marine sediments: Climate evolution during the Devonian. *Chemical Geology*, *246*(1–2), 19–38. https://doi.org/10.1016/j.chemgeo.2007.08.014

Sonnenberg, S. A., Theloy, C., & Jin, H. (2017). The Giant Continuous Oil Accumulation in the Bakken Petroleum System, U.S. Williston Basin. *Giant Fields of the Decade 2000–2010*. doi:10.1306/13572002m113508

Strauss, H. (1999). Geological evolution from isotope proxy signals — sulfur. *Chemical Geology*, *161*(1–3), 89–101. https://doi.org/10.1016/s0009-2541(99)00082-0

Torres, W. R., Díaz Nieto, C. H., Prévoteau, A., Rabaey, K., & Flexer, V. (2020). Lithium carbonate recovery from brines using membrane electrolysis. *Journal of Membrane Science*, *615*, 118416. https://doi.org/10.1016/j.memsci.2020.118416

Vorlicek, T. P., & Helz, G. R. (2002). Catalysis by mineral surfaces. *Geochimica et Cosmochimica Acta*, *66*(21), 3679–3692. https://doi.org/10.1016/s0016-7037(01)00837-7

Walker, J. C. G. (1986). Global geochemical cycles of carbon, sulfur and oxygen. *Marine Geology*, *70*(1–2), 159–174. https://doi.org/10.1016/0025-3227(86)90093-9

Waser, N. A. D., Harrison, P. J., Nielsen, B., Calvert, S. E., & Turpin, D. H. (1998). Nitrogen isotope fractionation during the uptake and assimilation of nitrate, nitrite, ammonium, and urea by a marine diatom. *Limnology and Oceanography*, *43*(2), 215–224. https://doi.org/10.4319/lo.1998.43.2.0215

Xu, J. (2020, January 11). *Depositional and chemical controls on sedimentation, sequence stratigraphy, and pore development of the Pronghorn, Lower Silt, and Lower Shale members of the Bakken Formation, Williston Basin*. Mountainscholar. https://mountainscholar.org/handle/11124/173107

Zheng, Y., Anderson, R. F., van Geen, A., & Fleisher, M. Q. (2002). Preservation of particulate non-lithogenic uranium in marine sediments. *Geochimica et Cosmochimica Acta*, *66*(17), 3085–3092. https://doi.org/10.1016/s0016-7037(01)00632-9

Zheng, Y., Anderson, R. F., van Geen, A., & Kuwabara, J. (2000). Authigenic molybdenum formation in marine sediments: a link to pore water sulfide in the Santa Barbara Basin. *Geochimica et Cosmochimica Acta*, *64*(24), 4165–4178. https://doi.org/10.1016/s0016-7037(00)00495-6